Predicting the EGFR Mutation Status of Lung Adenocarcinoma Manifesting as Ground-glass Nodules Based on ^{18}F-FDG PET/CT Radiomics

Yunmei Shi
Third Affiliated Hospital of Soochow University: Changzhou First People's Hospital
Rong Niu
Third Affiliated Hospital of Soochow University: Changzhou First People's Hospital
Jianxiong Gao
Third Affiliated Hospital of Soochow University: Changzhou First People's Hospital
Xiaoliang Shao
Third Affiliated Hospital of Soochow University: Changzhou First People's Hospital
Jianfeng Wang
Third Affiliated Hospital of Soochow University: Changzhou First People's Hospital
Feifei Zhang
Third Affiliated Hospital of Soochow University: Changzhou First People's Hospital
Yuetao Wang
Third Affiliated Hospital of Soochow University: Changzhou First People's Hospital
https://orcid.org/0000-0003-2859-8625
Xiaonan Shao (scorey@sina.com)
Third Affiliated Hospital of Soochow University: Changzhou First People's Hospital

Research Article

Keywords: ground-glass nodules, lung adenocarcinoma, epidermal growth factor receptor, radiomics, machine learning, positron emission tomography

Posted Date: February 15th, 2022

DOI: https://doi.org/10.21203/rs.3.rs-1329422/v1

Abstract

Background: The incidence of ground-glass nodules (GGNs) in epidermal growth factor receptor (EGFR)-mutated lung adenocarcinoma is significantly higher. For multiple GGNs, invasive detection is difficult to achieve. Therefore, there is an urgent need for an ideal non-invasive examination method to predict the EGFR mutation status in GGNs patients. Radiomics-based machine learning (ML) has been applied in various tumors. However, no predictive models based on ^{18}F-FDG PET/CT radiomics features have been used to identify the EGFR mutation status in lung adenocarcinoma manifesting as GGNs. We amied to explore the predictive value of combining ^{18}F-FDG PET/CT based radiomics and ML methods in distinguishing the mutation status of EGFR in lung adenocarcinoma manifesting as GGNs.

Results: Among the 106 nodules, 81 had EGFR mutations (76.4%). There were no significant differences in general data, morphological characteristics, and PET/CT parameters between the EGFR mutation group and the wild group (P>0.05). Among the four models in the test set, XGBoost showed the best performance (AUC=0.798, 95%CI: 0.627-0.904) and was significantly better than Random Forest (AUC=0.680, 95%CI: 0.509-0.822) (Z=2.122, P=0.034).

Conclusion: The combination of ^{18}F-FDG PET/CT radiomics and machine learning methods is a potential non-invasive method for predicting the EGFR mutation status of GGNs lung adenocarcinoma.

Introduction

With the widespread application of low-dose CT in lung cancer screening, lung ground-glass nodules (GGNs) detection rate continues to increase, especially in the non-smoking young women in Asia, and the incidence of multiple GGNs is rising (1, 2). GGNs can be divided into pure ground-glass nodules (pGGN) and mixed ground-glass nodules (mGGN). Surgical resection is recommended for the highly suspicious and persistent single GGN. However, for patients with multiple GGNs or intolerable physical conditions, invasive fine-needle aspiration biopsy or surgery cannot be performed, and targeted adjuvant treatment is usually recommended.

Studies have shown that the progression-free survival of lung cancer patients with epidermal growth factor receptor (EGFR) mutation was significantly extended after EGFR tyrosine kinase inhibitors (TKIs) treatment (3, 4), and TKIs have become the first-line drug for NSCLC treatment. So far, the EGFR mutation is mainly detected by invasive detection methods such as surgery or needle biopsy. These methods have many limitations, such as sampling deviation caused by tumor heterogeneity, related complications caused by invasive biopsy, and the low detection speed and high cost. Moreover, invasive detection may yield false-negative results due to insufficient sampling quantity or quality (5, 6). For multiple GGNs, invasive detection is even more difficult to achieve, making patients lose the potential opportunity for EGFR-TKIs treatment. Previous studies (7–9) have also shown that the incidence of GGNs in EGFR-mutated lung adenocarcinoma is significantly higher. Therefore, there is an urgent need for an ideal non-invasive examination method to predict the EGFR mutation status in GGNs patients.

As a non-invasive imaging method, ^{18}F-deoxyglucose (FDG) PET/CT has been widely used in tumor diagnosis, efficacy assessment, and prognostic evaluation (10). In recent years, many studies have explored the relationship between the parameters of chest CT or ^{18}F-FDG PET/CT and the EGFR mutation status, but the results are controversial (11–16), which may be related to intertumoral heterogeneity. Due to the advantages of non-invasiveness, high-speed, low cost, and simple operation (17), radiomics has become an important tool for studying tumor heterogeneity, and it has shown great potential in predicting the clinical outcomes and genomic characteristics (18). So far, the studies using radiomic features to predict EGFR mutation status of GGNs lung adenocarcinoma are all based on chest CT images (19–21), which can only provide tumor morphological information. No predictive models based on ^{18}F-FDG PET/CT radiomics features have been used to identify the EGFR mutation status in lung adenocarcinoma manifesting as ground-glass nodules.

Radiomics-based machine learning (ML) has been applied in histology classification, treatment response, and prognostic prediction for various tumors (23–26). Studies have confirmed that the combination of radiomics and ML methods has superior diagnostic performance in the differentiation of benign and malignant GGN and predicting histological subtypes of non-small cell lung cancer (20, 27). Therefore, this study aims to combine the radiomic features of ^{18}F-FDG PET/CT with ML methods to develop and validate a predictive model that can effectively identify the EGFR mutation status in GGNs lung adenocarcinoma. We hope the model can provide a reference for the non-invasive prediction of EGFR mutation status in GGNs patients.

Materials And Methods

1. Study subject

A retrospective analysis was performed on patients who underwent ^{18}F-FDG PET/CT examination from November 2017 to April 2021 in the Third Affiliated Hospital of Soochow University. The patients received surgical resection and EGFR detection within one month after PET/CT examination. Lung adenocarcinoma was confirmed by pathology after surgery. According to the EGFR detection results, the patients were divided into mutant and wild-type groups. The inclusion criteria were: (1) lung cancer was manifesting as GGNs by imaging; (2) PET/CT and HRCT examinations were performed within one month before surgery; (3) lung adenocarcinoma was confirmed by postoperative pathology, and EGFR mutation status was measured. The exclusion criteria were: (1) Poor image quality of GGNs or lesions were difficult to segment; (2) Patients with other tumors; (3) Patients with severe liver disease or diabetes; (4) The FDG uptake of GGNs was too low to distinguish it from the lung background. Finally, 106 patients were enrolled, including 106 GGNs, of which 81 were EGFR mutants, and 25 were wild-type (Figure 1). This study has been approved by the Ethics Committee of the Third Affiliated Hospital of Soochow University [Approval Number: (2020) Section No. 075].

2. EGFR mutation analysis

EGFR mutation analysis was performed by experienced pathologists in our pathology department using postoperative samples. The slice thickness was 3-5 mm, and the samples were frozen for 30 minutes. Gene amplification was performed using the ARMS method, also known as allele-specific amplification. Exon 18, 19, 20, and 21 of EGFR gene were tested using the Shanghai Yuanqi EGFR gene mutation detection kit (AmoyDx EGFR mutation detection kit), and the result was interpreted according to the criteria provided by the test kit.

3. Radiomics analysis

The radiomics analysis consists of 6 steps. The details are shown in Figure 2. and explained in detail as follows.

Image Acquisition

The image acquisition protocol was based on the Imaging Biomarker Standardization Initiative (IBSI) reporting guidelines (28). Within one month before surgery, the patients received ^{18}F-FDG PET/CT examination (Biograph mCT 64, Siemens, Erlangen, Germany). According to the European Association for Nuclear Medicine (EANM) guideline 1.0 (version 2.0 released in February 2015) (29), the patients were fasted for 4 to 6 hours and then received an intravenous injection of ^{18}F-FDG at 3.70 to 5.55 MBq/kg for imaging. The images were collected after 60 minutes of rest. All patients lay supine; the collection time was 2 min/bed, and the collection range was from the skull base to the middle femur. After PET/CT, the images were reconstructed on the post-processing workstation (TrueD software), and a spiral CT scan was immediately performed on GGNs under a breath-holding state. The scanning and reconstruction parameters were: tube voltage 140 kV; tube current was automatically adjusted by the caredose software according to human anatomy and tissue density; rotation time 0.5 s/turn; pitch 0.6; layer thickness 3.0mm; matrix 512×512; lung window: window width 1200 HU, window level -600 HU; mediastinal window: window width 350 HU, window level 40 HU. The images were reconstructed based on 1.0 mm layer thickness and 0.5 mm layer spacing. Attenuation correction was performed on the PET image using CT data, and the corrected PET image was combined with the CT image. No respiratory gating technology was applied during image acquisition.

Image segmentation

3D-Slicer (version number 4.11.20200930, www.slicer.com) was used for image segmentation. We used a semi-automatic segmentation method developed by Beichel et al. (30) for PET images. For CT images (3mm), we used NVIDIA AI-Assisted Annotation (3D-Slicer built-in) and boundary-based CT segmentation model to process lung nodule images. The above segmentation was verified by experienced nuclear medicine doctors blinded to the patient's pathology and EGFR mutation status.

Image Preprocessing

Before feature extraction, the images were normalized and interpolated (sitkBSpline algorithm, B-spline of order 3 interpolation) so that the isotropic voxel spacing was ration invariant. Feature extraction was performed to compare the image data from different samples. The CT image was resampled to size 1 mm × 1 mm × 1 mm, and the PET image was resampled to size 3 mm × 3 mm × 3 mm. The images were discretized by the fixed binwidth method. The binwidth of CT and PET images were 25 and 0.313, respectively. Discretization, Laplacian of Gaussian (LOG), and wavelet transform preprocessing were performed to generate different feature sets. Different sigma values were used for the LOG filter to extract fine, medium, and coarse features, ranging from 0.5 to 5, with a step size of 0.5 (31). The wavelet transform produced 8 decompositions per level (applying all possible combinations of high- or low-pass filters in each of the three dimensions, including HHH, HHL, HLH, HLL, LHH, LHL, LLH, and LLL). Preprocessing steps (including discretization, LOG, and wavelet transform) were performed on all shape features, first-order statistics, and textural features.

Feature Extraction

In the next step, multiple features from different feature classes were extracted. These categories included shape and morphological features (14 shape features), first-order statistics (18 FOS features), gray-level co-occurrence matrix (24 GLCM features), gray-level dependence matrix (14 GLDM features), gray-level run length matrix (16 GLRLM features), gray-level scale zone matrix (16 GLSZM features), and neighboring gray tone difference matrix (5 NGTDM features). The open-source Python (3.7.10) library PyRadiomics (version number 3.0.1, https://pyradiomics.readthedocs.io/en/latest/#) was used for image feature extraction (32). The radiomic features calculated by this package conform to the definition of features described by the Image Biomarker Standardization Initiative (IBSI), which ensures the coordination and reproducibility of the calculated radiological features, thereby promoting the reproducibility of this study (32,33). The detailed information of the radiomic features was listed in Supplementary Material Table S1.

Feature Selection

Due to a large number of radiomic features and the relatively small case number in this study, the variance method was used to remove features with small variance (threshold=0.18) to avoid overfitting the model. Subsequently, the data set was stratified random sampled at a ratio of 65:35 to generate training set (n=68) and testing set (n=38). In the training set, the Mann-Whitney U test was used to screen out 55 radiomic features (p-value<0.1) related to the mutation status of EGFR. Then, in the standardized training set, the Least Absolute Shrinkage and Selection Operator (LASSO) algorithm selected the optimal 14 predictive features from the 55 features (34). The LASSO algorithm adds an L1 regularization term to a least square algorithm to avoid overfitting, and 5-fold cross-validation was used. The Spearman correlation matrix of the selected 14 radiomic features was calculated (Supplementary Material Figure S1), and the highly correlated redundant features (r>0.85) were examined.

Classifier and Modeling

The analysis was performed using the internally developed Python framework in the open-source Python library Scikit-Learn (35), including feature selection and classification. The selected 14 predictive features were used to train the four ML models, including Logistic Regression (LR), Random Forest (RF), Support Vector Machine (SVM), and Extreme gradient boosting (XGBoost). The StratifiedKFold iterator in scikit-learn was used to apply 5-fold cross-validation in the training set to determine the model generalization. StratifiedKFold is a variation of k-fold cross-validation. It ensures that each set contains approximately the same percentage of samples of each target class as the whole training dataset. The AUC of the estimator applicable to the imbalance classification was used to evaluate the parameter settings.

4. Statistical analysis

The R software (version 3.4.3; http://www.R-project.org/) was used for statistical analysis. Continuous variables were expressed as mean ± standard deviation (normal distribution) or median (Q1-Q3) (skew distribution); categorical variables were expressed as frequency or rate (%). χ^2 test (categorical variable), T-test (normal distribution), or Mann-Whitney U test (skew distribution) was used to compare the differences in general data and PET/CT conventional parameters between different EGFR mutation states (binary categorical variables). To test the model's generalization ability, 5-fold cross-validation was performed on the model based on the selected features. The receiver operating characteristic (ROC) curve and AUC were applied on the testing set to evaluate the model performance, provide classification report and confusion matrix, and calculate sensitivity, specificity, accuracy, positive prediction value (PPV), and negative prediction value (NPV), which provided quantitative performance measure of the model. Pairwise comparison of the AUCs of the models was performed using the method proposed by Delong et al. (36), and a calibration curve was drawn to compare the prediction accuracy of the models. All statistical tests were two-sided, and $P<0.05$ was considered statistically significant.

Results

1. Comparison of the general data, morphological characteristics, and PET/CT routine parameters of the two groups

A total of 106 GGNs from 106 patients were included in this study, including 31 males and 75 females, with an average age of 63.9 ± 9.3 years old (range: 38-82 years old). There were 81 cases with EGFR mutations (76.4%), of which 27 cases had exon 19 deletion, 1 case had exon 20 mutation, and 53 cases had exon 21 mutation. The comparison between groups showed that the proportion of women in mutant group was higher than that in wild-type group (75.3% vs. 56.0%), but the difference was not significant (P=0.064). There was no significant difference in smoking history (P=0.995). Moreover, the GGO number, nodule type (pGGN and mGGN), location, shape, morphological characteristics (lobulated, spiculation, bronchial sign, cystic appearance, pleural depression sign), and PET/CT routine parameters (D_{GGN}, D_{Solid}, CTR, CT_{GGO}, SUVmax, SUV index) were not significantly different between the two groups (P=0.113-0.996) (Table 1).

Table 1
Comparison of general data and imaging parameters between EGFR mutant and wild-type group

EGFR classification	Wild-type group	Mutant group	P-value
N	25	81	
Age (years)	62.1 ± 9.0	64.5 ± 9.3	0.260
Gender			0.064
Female	14 (56.0%)	61 (75.3%)	
Male	11 (44.0%)	20 (24.7%)	
Fasting blood glucose (mmol/L)	6.18 ± 1.94	6.00 ± 1.08	0.561
Smoking history	4 (16.0%)	13 (16.1%)	0.995
GGO number	1.0 (1.0-2.0)	2.0 (1.0-4.0)	0.075
Nodule type			0.656
pGGN	2 (8.0%)	9 (11.1%)	
mGGN	23 (92.0%)	72 (88.9%)	
Location			0.308
Up right	6 (24.0%)	34 (42.0%)	
Middle right	3 (12.0%)	4 (4.9%)	
Low right	3 (12.0%)	10 (12.4%)	
Up left	7 (28.0%)	23 (28.4%)	
Low left	6 (24.0%)	10 (12.4%)	
Shape			0.411
Circular/ellipse	15 (60.0%)	41 (50.6%)	
Polygon/irregular	10 (40.0%)	40 (49.4%)	
Lobulated	16 (64.0%)	60 (74.1%)	0.328
Spiculation	14 (56.0%)	57 (70.4%)	0.182
Bronchial sign	23 (92.0%)	74 (91.4%)	0.920
Cystic appearance	9 (36.0%)	17 (21.0%)	0.127
Pleural depression sign	17 (68.0%)	67 (82.7%)	0.113
D_{GGN} (mm)	28.4 ± 11.4	26.0 ± 8.6	0.248

EGFR classification	Wild-type group	Mutant group	P-value
D_{Solid} (mm)	12.0 (6.7-15.4)	13.5 (6.0-18.3)	0.612
CTR	0.44 (0.3-0.7)	0.51 (0.3-0.7)	0.996
CT_{GGO}	-504.2 ± 127.2	-473.7 ± 111.6	0.251
SUVmax	2.9 (1.8-4.6)	3.1 (2.2-4.4)	0.843
SUV index	1.20 (0.8-1.8)	1.20 (0.9-1.7)	0.876

Note: D_{GGN}: Nodule diameter; D_{solid}: diameter of solid component in nodule; CTR: D_{solid}/D_{GGN}; CT_{GGO}: CT value of ground-glass opacity; SUVindex: ratio of the nodule SUVmax to liver SUVmean

2. Screening of radiomic features

A total of 3562 quantitative features (1781 PET features, 1781 CT features) were extracted from each segmented tumor region. 1559 features were screened out first using the variance method, including 1049 PET features and 510 CT features. Then, the data set was randomly sampled in layers at a 65:35 ratio to generate training set (68 cases, 16 negative cases, and 52 positive cases) and testing set (38 cases, 9 negative cases, and 29 positive cases).

Fifty-five features (14 PET features, 41 CT features) were selected using the Mann-Whitney U test (threshold value 0.1) in the training set. After data standardization, LASSO screening (CV=5) was performed. The best lambda value was 0.039, and 14 features (2 PET features and 12 CT features) were eventually selected (Figure 3). Including PET: 1 gray scale area matrix (GLSZM) feature, 1 first-order statistics (FOS) feature, CT: 1 FOS feature, 2 grayscale dependency matrix (GLDM) features, 8 Grayscale size region matrix (GLSZM) features, 1 grayscale runlength matrix (GLRLM) feature.

3. Radiomics modeling

The 14 features selected by LASSO were used to train the four ML models. The training parameters of the model and the 5-fold cross-validation results are shown in Supplementary Material Table S2 and Figure S2. It can be seen that in the training set, except for LR (average AUC=0.936), RF, SVM, and XGBoost all achieved perfect fitting (average AUC=1.000), but this also means that there is a high risk of overfitting in the test set.

4. Evaluation of model efficacy

Table 2 shows the comprehensive performance comparison of the four classifiers on the test set. The AUC of XGBoost was the largest [0.789 (95%CI: 0.627-0.904)], and the AUC of RF was the smallest [0.680 (95%CI: 0.509-0.822)]. It shows that there is serious overfitting in RF. Using the method proposed by Delong et al. to compare the ROC curves in pairs, it was found that the AUC of RF and XGBoost had significant differences (Z=2.122, P=0.034), and the remaining classifiers had no significant differences

between the two groups (P=0.132-0.822). The results were shown in Table 2 and Figure 4. The calibration curves of the four classifiers on the test set were compared in Supplementary Material Figure S3. It can be seen that the calibration of SVM was better.

Table 2
Performance comparison of the four models on the test set

Model	AUC (95%CI)	Accuracy	Sensitivity	Specificity	PPV	NPV	W:TN-FP	M:TP-FN
LR	0.693 (0.523 - 0.832)	0.711	0.759	0.556	0.846	0.417	5-4	22-7
RF	0.680 (0.509 - 0.822)	0.842	1.000	0.333	0.829	1.000	3-6	29-0
SVM	0.739 (0.572 - 0.868)	0.763	0.862	0.444	0.833	0.500	4-5	25-4
XGBoost	0.789 (0.627 - 0.904)	0.763	0.828	0.556	0.857	0.500	5-4	24-5

Note: PPV: positive prediction value; NPV: negative prediction value; W: wild-type; TN-FP: true negative - false positive; M: mutant-type; TP-FN: true positive - false negative; LR: Logistic Regression; RF: Random Forest; SVM: Support Vector Machine; XGBoost: extreme gradient boosting

Discussion

For multiple and unresectable GGNs, targeted therapy has become an effective treatment option. Although surgery or needle biopsy is currently the main method for detecting EGFR mutation status, they have many limitations(6). Thus, there is an urgent need for an ideal non-invasive examination method to predict EGFR mutation status. Compared with solid nodules, detecting EGFR mutation status in GGNs using PET/CT radiomics is a more challenging task. This study used 2 PET features and 12 CT features to construct four ML models (LR, RF, SVM, and XGBoost) to predict the EGFR mutation status of lung adenocarcinoma with GGNs. The results indicated that XGBoost showed the best performance. The combination of ^{18}F-FDG PET/CT based radiomics and ML methods might help predict EGFR mutation status in patients with GGNs lung adenocarcinoma. Therefore, our study provides a reference to help to determine the treatment strategy for inoperable persistent single/multiple GGNs lung adenocarcinomas.

This study first investigated the relationship between ^{18}F-FDG uptake and EGFR mutation status. The results showed no significant difference in SUVmax and SUVindex between EGFR mutant and wild-type patients. Similarly, Lee et al. (15) and Caicedo et al. (37) also showed no significant difference in SUVmax between the EGFR wild group and the mutant group of NSCLC. However, some studies reported that the

uptake of ^{18}F-FDG by NSCLC with EGFR mutation was lower than wild-type (12, 14). Ko et al. (38) and Kanmaz et al. (39) found that the SUVmax of EGFR-mutant lung adenocarcinoma was significantly higher than that of wild-type lung adenocarcinoma. The controversy between these studies may be due to the different TNM staging and histological types of the selected patients, and the above studies did not distinguish between solid and subsolid nodules. The different results indicate that SUVmax may not be a reliable marker for predicting EGFR mutation status.

Unlike SUVmax, radiomics analysis can reflect the potential spatial differences and heterogeneity of intratumoral voxel intensity and tracer uptake to describe tumor characteristics better. Rios Velazquez (40) and Sacconi (41) et al. tested the performance of using CT radiomic features to predict EGFR mutation status in lung cancer patients, and their AUCs were 0.69 and 0.56-0.75, respectively. Yip et al. (42) found that the AUC of PET radiomic model alone was 0.67. In contrast, the AUC of PET/CT radiomics based models from Zhang et al. (43) and Li et al. (44) were 0.79 and 0.80, respectively. The above studies show that the dual-modality radiomics model based on PET/CT has better predictive performance than the single mode. However, compared with the larger sample size of CT radiomics research, the current sample size of PET/CT radiomics is limited (45). Thus, the generalization ability of PET/CT radiomics based model needs to be further tested.

As a branch of artificial intelligence, machine learning has been widely used in medical research (22, 46). Studies have confirmed that the combination of radiomics and ML methods has superior diagnostic performance in several tumors (20, 25, 27, 47). The performance of various feature selection and ML algorithms in medical image classification has been studied in recent years to determine which feature selection and ML algorithms are suitable for the given medical image data. Shiri et al. (48) used six feature selection methods and 12 classifiers for multivariate prediction of gene mutation status and found multivariate ML-based AUC performances were up to 0.82 for EGFR. Wang et al. (49) explored the value of ML and 18F-FDG PET/CT radiomics features in predicting EGFR mutation subtypes in patients with lung adenocarcinoma. They found the predictive performance of mean PET/CT feature-based model in EGFR mutation subtypes was better than PET feature-based model and CT feature-based model. Our study found that the XGBoost model had the best predictive performance. The AUC of XGBoost on testing set was 0.789. The XGBoost algorithm has provided reliable results for various medical applications and won numerous machine learning awards (50). It has been confirmed that the combination of radiomics and XGBoost is superior to other machine learning methods (20).

However, due to the numerous available feature selection methods and ML algorithms, there is no “one fits all” approach as performance of various ML workflows has been shown to depend on application and/or type of data (27, 51–53). It is not controversial that the combination of radiomics and ML methods is superior to traditional methods in distinguishing the mutation status of EGFR in lung adenocarcinoma manifesting as GGNs.

This study has the following limitations. First, this study is a retrospective single-center study, and patient selection might be biased. In the future, a multi-center study and external verification will be performed.

Second, GGNs with low FDG uptake were excluded from the study; thus, our model is unsuitable for such patients. New technologies such as super iteration may be needed to increase the uptake of imaging agent FDG by GGNs, or more specific EGFR-targeted imaging agents can be developed for clinic application. In addition, sample size is currently a common challenge for radiomics/genomics research because the analysis with small sample size is prone to overfitting due to the large numbers of radiomic features. Although cross-validation was used in this study, the problem of overfitting was still inevitable.

Conclusions

We confirmed the relationship between ^{18}F-FDG PET/CT radiomic features and the EGFR mutation status of GGNs lung adenocarcinoma. In this study, the prediction model constructed based on radiomics and ML methods can be used to distinguish the EGFR mutation status of persistent single or multiple GGNs lung adenocarcinomas. This non-invasive method can provide useful information for decision-making during clinical treatment.

Abbreviations

^{18}F-FDG = ^{18}F-fluorodeoxyglucose

AUC = area under the curve

CTR = consolidation-to-tumor ratio

CT_{GGO} = CT value of ground glass component of nodule

D_{solid} = diameter of solid component in nodule

EGFR = epidermal growth factor receptor

FOS = first-order statistics

GGN = ground-glass opacity nodule

GLCM = gray-level co-occurrence matrix

GLDM = gray-level dependence matrix

GLRLM = gray-level run length matrix

GLSZM = gray-level scale zone matrix

HRCT = high-resolution CT

LASSO = least absolute shrinkage sum selection operator

LOG = laplacian of gaussian

LR= Logistic Regression

NGTDM = neighboring gray tone difference matrix

NPV = negative prediction value

PET = positron emission tomography

PPV = positive prediction value

RF= Random Forest

ROC = receiver operating characteristic curve

SUV = standardized uptake value

SUVindex = ratio of the nodule SUVmax to liver SUVmean

SUVmax = maximum standardized uptake value

SVM= Support Vector Machine

XGBoost = extreme gradient boosting

Declarations

Ethics approval and consent to participate

All methods were carried out in accordance with relevant guidelines and regulations. This study has been approved by the Ethics Committee of the Third Affiliated Hospital of Soochow University [Approval Number: (2020) Section No. 075].

The need for informed consent from each patient was waived because of the retrospective design.

Consent for publication

Not applicable.

Availability of data and material

The datasets generated and/or analysed during the current study are available from the corresponding author on reasonable request.

Competing interests

The authors declare that they have no competing interests.

Funding

This study was supported by Key Laboratory of Changzhou High-tech Research Project (CM20193010); Young Talent Development Plan of Changzhou Health Commission (CZQM2020012); Changzhou Science and Technology Program (CJ20210063); Major Project of Changzhou Health Commission (ZD202109).

Authors' contributions

XS and YW contributed to the study concepts and the study design. YS, RN, JG, and XS contributed to data acquisition and reconstructions. XS, RN, XS, JW, and FZ contributed to data analyses and interpretation. XS contributed to the statistical analysis. XS, YS, and YW contributed to the manuscript preparation, editing, and review. All authors read and approved the final manuscript.

Acknowledgements

Not applicable.

References

1. Niu R, Wang Y, Shao X, Jiang Z, Wang J, Shao X. Association Between (18)F-FDG PET/CT-Based SUV Index and Malignant Status of Persistent Ground-Glass Nodules. Front Oncol 2021;11:594693.
2. Gould MK, Donington J, Lynch WR, Mazzone PJ, Midthun DE, Naidich DP, Wiener RS. Evaluation of individuals with pulmonary nodules: when is it lung cancer? Diagnosis and management of lung cancer, 3rd ed: American College of Chest Physicians evidence-based clinical practice guidelines. Chest 2013;143:e93S-e120S.
3. Recondo G, Facchinetti F, Olaussen KA, Besse B, Friboulet L. Making the first move in EGFR-driven or ALK-driven NSCLC: first-generation or next-generation TKI? Nat Rev Clin Oncol 2018;15:694-708.
4. da Cunha Santos G, Shepherd FA, Tsao MS. EGFR mutations and lung cancer. Annu Rev Pathol 2011;6:49-69.
5. Ellison G, Zhu G, Moulis A, Dearden S, Speake G, McCormack R. EGFR mutation testing in lung cancer: a review of available methods and their use for analysis of tumour tissue and cytology samples. J Clin Pathol 2013;66:79-89.
6. Taniguchi K, Okami J, Kodama K, Higashiyama M, Kato K. Intratumor heterogeneity of epidermal growth factor receptor mutations in lung cancer and its correlation to the response to gefitinib. Cancer Sci 2008;99:929-35.
7. Liu Y, Kim J, Qu F, Liu S, Wang H, Balagurunathan Y, Ye Z, Gillies RJ. CT Features Associated with Epidermal Growth Factor Receptor Mutation Status in Patients with Lung Adenocarcinoma. Radiology 2016;280:271-80.

8. Hasegawa M, Sakai F, Ishikawa R, Kimura F, Ishida H, Kobayashi K. CT Features of Epidermal Growth Factor Receptor-Mutated Adenocarcinoma of the Lung: Comparison with Nonmutated Adenocarcinoma. J Thorac Oncol 2016;11:819-26.
9. Cao Y, Xu H. A new predictive scoring system based on clinical data and computed tomography features for diagnosing EGFR-mutated lung adenocarcinoma. Curr Oncol 2018;25:e132-e8.
10. Ettinger DS, Wood DE, Aisner DL, Akerley W, Bauman J, Chirieac LR, D'Amico TA, DeCamp MM, Dilling TJ, Dobelbower M, Doebele RC, Govindan R, Gubens MA, Hennon M, Horn L, Komaki R, Lackner RP, Lanuti M, Leal TA, Leisch LJ, Lilenbaum R, Lin J, Loo BW, Jr., Martins R, Otterson GA, Reckamp K, Riely GJ, Schild SE, Shapiro TA, Stevenson J, Swanson SJ, Tauer K, Yang SC, Gregory K, Hughes M. Non-Small Cell Lung Cancer, Version 5.2017, NCCN Clinical Practice Guidelines in Oncology. J Natl Compr Canc Netw 2017;15:504-35.
11. Lee EY, Khong PL, Lee VH, Qian W, Yu X, Wong MP. Metabolic phenotype of stage IV lung adenocarcinoma: relationship with epidermal growth factor receptor mutation. Clin Nucl Med 2015;40:e190-5.
12. Cho A, Hur J, Moon YW, Hong SR, Suh YJ, Kim YJ, Im DJ, Hong YJ, Lee HJ, Kim YJ, Shim HS, Lee JS, Kim JH, Choi BW. Correlation between EGFR gene mutation, cytologic tumor markers, 18F-FDG uptake in non-small cell lung cancer. BMC Cancer 2016;16:224.
13. Yoshida T, Tanaka H, Kuroda H, Shimizu J, Horio Y, Sakao Y, Inaba Y, Iwata H, Hida T, Yatabe Y. Standardized uptake value on (18)F-FDG-PET/CT is a predictor of EGFR T790M mutation status in patients with acquired resistance to EGFR-TKIs. Lung Cancer 2016;100:14-9.
14. Lv Z, Fan J, Xu J, Wu F, Huang Q, Guo M, Liao T, Liu S, Lan X, Liao S, Geng W, Jin Y. Value of (18)F-FDG PET/CT for predicting EGFR mutations and positive ALK expression in patients with non-small cell lung cancer: a retrospective analysis of 849 Chinese patients. Eur J Nucl Med Mol Imaging 2018;45:735-50.
15. Lee SM, Bae SK, Jung SJ, Kim CK. FDG uptake in non-small cell lung cancer is not an independent predictor of EGFR or KRAS mutation status: a retrospective analysis of 206 patients. Clin Nucl Med 2015;40:950-8.
16. Ruan M, Liu L, Wang L, Lei B, Sun X, Chang C, Shen Y, Xie W. Correlation between combining (18)F-FDG PET/CT metabolic parameters and other clinical features and ALK or ROS1 fusion in patients with non-small-cell lung cancer. 2020;47:1183-97.
17. Yip SS, Aerts HJ. Applications and limitations of radiomics. Phys Med Biol 2016;61:R150-66.
18. Lambin P, Leijenaar RTH, Deist TM, Peerlings J, de Jong EEC, van Timmeren J, Sanduleanu S, Larue R, Even AJG, Jochems A, van Wijk Y, Woodruff H, van Soest J, Lustberg T, Roelofs E, van Elmpt W, Dekker A, Mottaghy FM, Wildberger JE, Walsh S. Radiomics: the bridge between medical imaging and personalized medicine. Nat Rev Clin Oncol 2017;14:749-62.
19. Yang X, Dong X, Wang J, Li W, Gu Z, Gao D, Zhong N, Guan Y. Computed Tomography-Based Radiomics Signature: A Potential Indicator of Epidermal Growth Factor Receptor Mutation in Pulmonary Adenocarcinoma Appearing as a Subsolid Nodule. Oncologist 2019;24:e1156-e64.

20. Hu X, Gong J, Zhou W, Li H, Wang S, Wei M, Peng W, Gu Y. Computer-aided diagnosis of ground glass pulmonary nodule by fusing deep learning and radiomics features. Phys Med Biol 2021;66:065015.
21. Meng F, Guo Y, Li M, Lu X, Wang S, Zhang L, Zhang H. Radiomics nomogram: A noninvasive tool for preoperative evaluation of the invasiveness of pulmonary adenocarcinomas manifesting as ground-glass nodules. Transl Oncol 2021;14:100936.
22. Choy G, Khalilzadeh O, Michalski M, Do S, Samir AE, Pianykh OS, Geis JR, Pandharipande PV, Brink JA, Dreyer KJ. Current Applications and Future Impact of Machine Learning in Radiology. Radiology 2018;288:318-28.
23. Ha S, Choi H, Cheon GJ, Kang KW, Chung JK, Kim EE, Lee DS. Autoclustering of Non-small Cell Lung Carcinoma Subtypes on (18)F-FDG PET Using Texture Analysis: A Preliminary Result. Nucl Med Mol Imaging 2014;48:278-86.
24. Zhou Y, Ma XL, Zhang T, Wang J, Zhang T, Tian R. Use of radiomics based on (18)F-FDG PET/CT and machine learning methods to aid clinical decision-making in the classification of solitary pulmonary lesions: an innovative approach. 2021.
25. Toyama Y, Hotta M, Motoi F, Takanami K, Minamimoto R, Takase K. Prognostic value of FDG-PET radiomics with machine learning in pancreatic cancer. Sci Rep 2020;10:17024.
26. Nasief H, Zheng C, Schott D, Hall W, Tsai S, Erickson B, Allen Li X. A machine learning based delta-radiomics process for early prediction of treatment response of pancreatic cancer. NPJ Precis Oncol 2019;3:25.
27. Han Y, Ma Y, Wu Z, Zhang F, Zheng D, Liu X, Tao L, Liang Z, Yang Z, Li X, Huang J, Guo X. Histologic subtype classification of non-small cell lung cancer using PET/CT images. Eur J Nucl Med Mol Imaging 2021;48:350-60.
28. Zwanenburg A, Leger S, Vallières M, Löck S. Image biomarker standardisation initiative. arXiv preprint arXiv:161207003 2016.
29. Boellaard R, Delgado-Bolton R, Oyen WJ, Giammarile F, Tatsch K, Eschner W, Verzijlbergen FJ, Barrington SF, Pike LC, Weber WA. FDG PET/CT: EANM procedure guidelines for tumour imaging: version 2.0. European journal of nuclear medicine and molecular imaging 2015;42:328-54.
30. Beichel RR, Van Tol M, Ulrich EJ, Bauer C, Chang T, Plichta KA, Smith BJ, Sunderland JJ, Graham MM, Sonka M, Buatti JM. Semiautomated segmentation of head and neck cancers in 18F-FDG PET scans: A just-enough-interaction approach. Med Phys 2016;43:2948-64.
31. Ganeshan B, Panayiotou E, Burnand K, Dizdarevic S, Miles K. Tumour heterogeneity in non-small cell lung carcinoma assessed by CT texture analysis: a potential marker of survival. Eur Radiol 2012;22:796-802.
32. van Griethuysen JJM, Fedorov A, Parmar C, Hosny A, Aucoin N, Narayan V, Beets-Tan RGH, Fillion-Robin JC, Pieper S, Aerts H. Computational Radiomics System to Decode the Radiographic Phenotype. Cancer Res 2017;77:e104-e7.
33. Zwanenburg A, Leger S, Vallières M, Löck S. Image biomarker standardisation initiative. arXiv. arXiv preprint arXiv:161207003 2016.

34. Kirienko M, Cozzi L, Rossi A, Voulaz E, Antunovic L, Fogliata A, Chiti A, Sollini M. Ability of FDG PET and CT radiomics features to differentiate between primary and metastatic lung lesions. 2018;45:1649-60.
35. Pedregosa F, Varoquaux G, Gramfort A, Michel V, Thirion B, Grisel O, Blondel M, Prettenhofer P, Weiss R, Dubourg V. Scikit-learn: Machine learning in Python. the Journal of machine Learning research 2011;12:2825-30.
36. DeLong ER, DeLong DM, Clarke-Pearson DL. Comparing the areas under two or more correlated receiver operating characteristic curves: a nonparametric approach. Biometrics 1988;44:837-45.
37. Caicedo C, Garcia-Velloso MJ, Lozano MD, Labiano T, Vigil Diaz C, Lopez-Picazo JM, Gurpide A, Zulueta JJ, Richter Echevarria JA, Perez Gracia JL. Role of [¹⁸F]FDG PET in prediction of KRAS and EGFR mutation status in patients with advanced non-small-cell lung cancer. Eur J Nucl Med Mol Imaging 2014;41:2058-65.
38. Ko KH, Hsu HH, Huang TW, Gao HW, Shen DH, Chang WC, Hsu YC, Chang TH, Chu CM, Ho CL, Chang H. Value of ¹⁸F-FDG uptake on PET/CT and CEA level to predict epidermal growth factor receptor mutations in pulmonary adenocarcinoma. Eur J Nucl Med Mol Imaging 2014;41:1889-97.
39. Kanmaz ZD, Aras G, Tuncay E, Bahadır A, Kocatürk C, Yaşar ZA, Öz B, Özkurt C, Gündoğan C, Çermik TF. Contribution of ¹⁸Fluorodeoxyglucose positron emission tomography uptake and TTF-1 expression in the evaluation of the EGFR mutation in patients with lung adenocarcinoma. Cancer Biomark 2016;16:489-98.
40. Rios Velazquez E, Parmar C, Liu Y, Coroller TP, Cruz G, Stringfield O, Ye Z, Makrigiorgos M, Fennessy F, Mak RH, Gillies R, Quackenbush J, Aerts H. Somatic Mutations Drive Distinct Imaging Phenotypes in Lung Cancer. Cancer Res 2017;77:3922-30.
41. Sacconi B, Anzidei M, Leonardi A, Boni F, Saba L, Scipione R, Anile M, Rengo M, Longo F, Bezzi M, Venuta F, Napoli A, Laghi A, Catalano C. Analysis of CT features and quantitative texture analysis in patients with lung adenocarcinoma: a correlation with EGFR mutations and survival rates. Clin Radiol 2017;72:443-50.
42. Yip SS, Kim J, Coroller TP, Parmar C, Velazquez ER, Huynh E, Mak RH, Aerts HJ. Associations Between Somatic Mutations and Metabolic Imaging Phenotypes in Non-Small Cell Lung Cancer. J Nucl Med 2017;58:569-76.
43. Zhang J, Zhao X, Zhao Y, Zhang J, Zhang Z, Wang J, Wang Y, Dai M, Han J. Value of pre-therapy (18)F-FDG PET/CT radiomics in predicting EGFR mutation status in patients with non-small cell lung cancer. Eur J Nucl Med Mol Imaging 2020;47:1137-46.
44. Li X, Yin G, Zhang Y, Dai D, Liu J, Chen P, Zhu L, Ma W, Xu W. Predictive Power of a Radiomic Signature Based on (18)F-FDG PET/CT Images for EGFR Mutational Status in NSCLC. Front Oncol 2019;9:1062.
45. Abdurixiti M, Nijiati M, Shen R, Ya Q, Abuduxiku N, Nijiati M. Current progress and quality of radiomic studies for predicting EGFR mutation in patients with non-small cell lung cancer using PET/CT images: a systematic review. Br J Radiol 2021;94:20201272.

46. Deo RC. Machine Learning in Medicine. Circulation 2015;132:1920-30.
47. Zheng J, Kong J, Wu S, Li Y, Cai J, Yu H, Xie W, Qin H, Wu Z, Huang J, Lin T. Development of a noninvasive tool to preoperatively evaluate the muscular invasiveness of bladder cancer using a radiomics approach. Cancer 2019;125:4388-98.
48. Shiri I, Maleki H, Hajianfar G, Abdollahi H, Ashrafinia S, Hatt M, Zaidi H, Oveisi M, Rahmim A. Next-Generation Radiogenomics Sequencing for Prediction of EGFR and KRAS Mutation Status in NSCLC Patients Using Multimodal Imaging and Machine Learning Algorithms. 2020;22:1132-48.
49. Wang Z, Ying G, Li X, Xu W. Value of machine learning and 18F-FDG PET/CT radiomics features in lung adenocarcinoma EGFR mutation subtypes prediction. Chinese Journal of Nuclear Medicine and Molecular Imaging 2021;41:479-85.
50. Livne M, Boldsen JK, Mikkelsen IK, Fiebach JB, Sobesky J, Mouridsen K. Boosted Tree Model Reforms Multimodal Magnetic Resonance Imaging Infarct Prediction in Acute Stroke. Stroke 2018;49:912-8.
51. Leger S, Zwanenburg A, Pilz K, Lohaus F, Linge A, Zöphel K, Kotzerke J, Schreiber A, Tinhofer I, Budach V, Sak A, Stuschke M, Balermpas P, Rödel C, Ganswindt U, Belka C, Pigorsch S, Combs SE, Mönnich D, Zips D, Krause M, Baumann M, Troost EGC, Löck S, Richter C. A comparative study of machine learning methods for time-to-event survival data for radiomics risk modelling. Sci Rep 2017;7:13206.
52. Shiri I, Maleki H, Hajianfar G, Abdollahi H, Ashrafinia S, Hatt M, Zaidi H, Oveisi M, Rahmim A. Next-Generation Radiogenomics Sequencing for Prediction of EGFR and KRAS Mutation Status in NSCLC Patients Using Multimodal Imaging and Machine Learning Algorithms. Mol Imaging Biol 2020;22:1132-48.
53. Deist TM, Dankers F, Valdes G, Wijsman R, Hsu IC, Oberije C, Lustberg T, van Soest J, Hoebers F, Jochems A, El Naqa I, Wee L, Morin O, Raleigh DR, Bots W, Kaanders JH, Belderbos J, Kwint M, Solberg T, Monshouwer R, Bussink J, Dekker A, Lambin P. Machine learning algorithms for outcome prediction in (chemo)radiotherapy: An empirical comparison of classifiers. Med Phys 2018;45:3449-59.

Figures

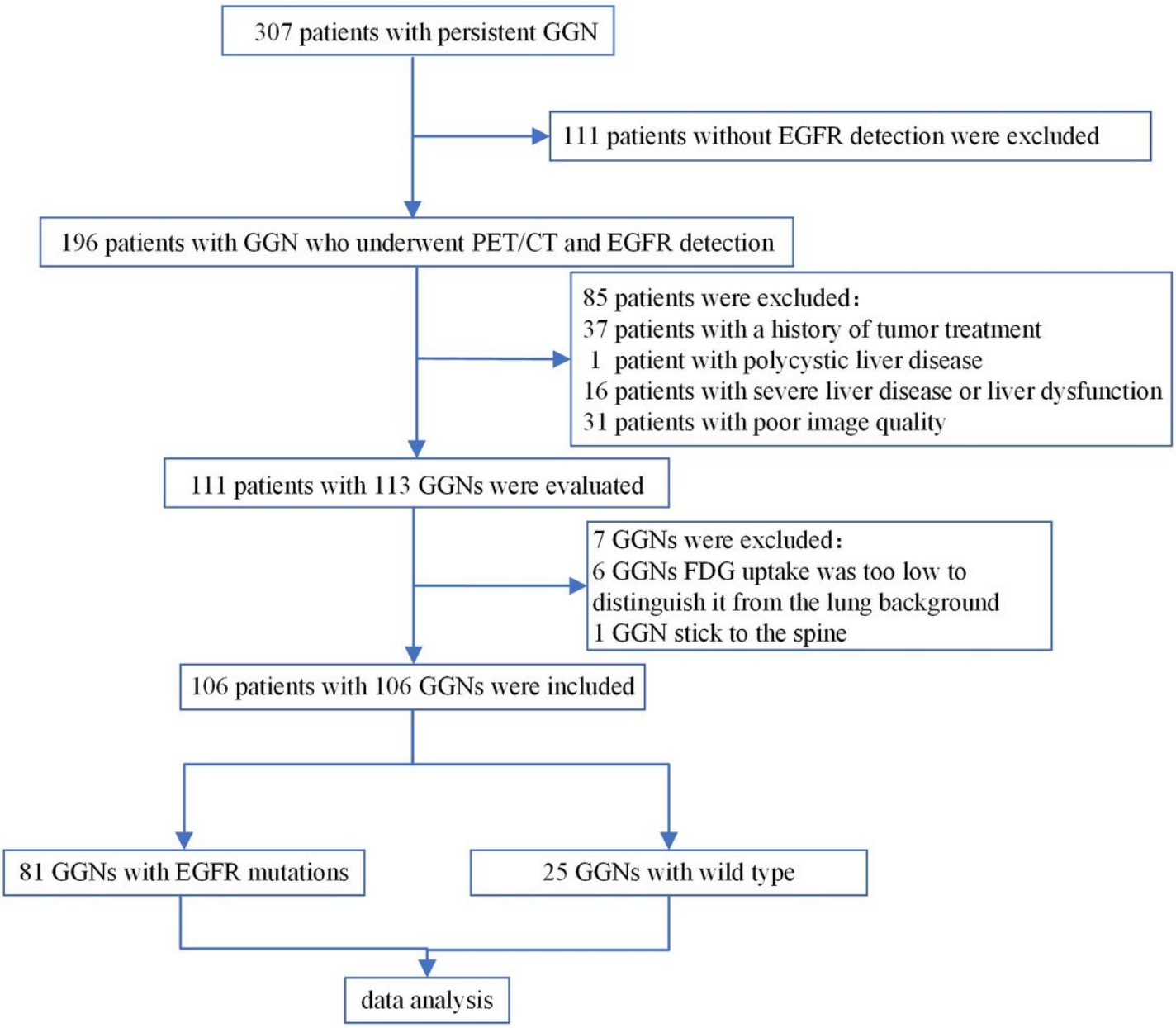

Figure 1

Flow chart of the study population selection

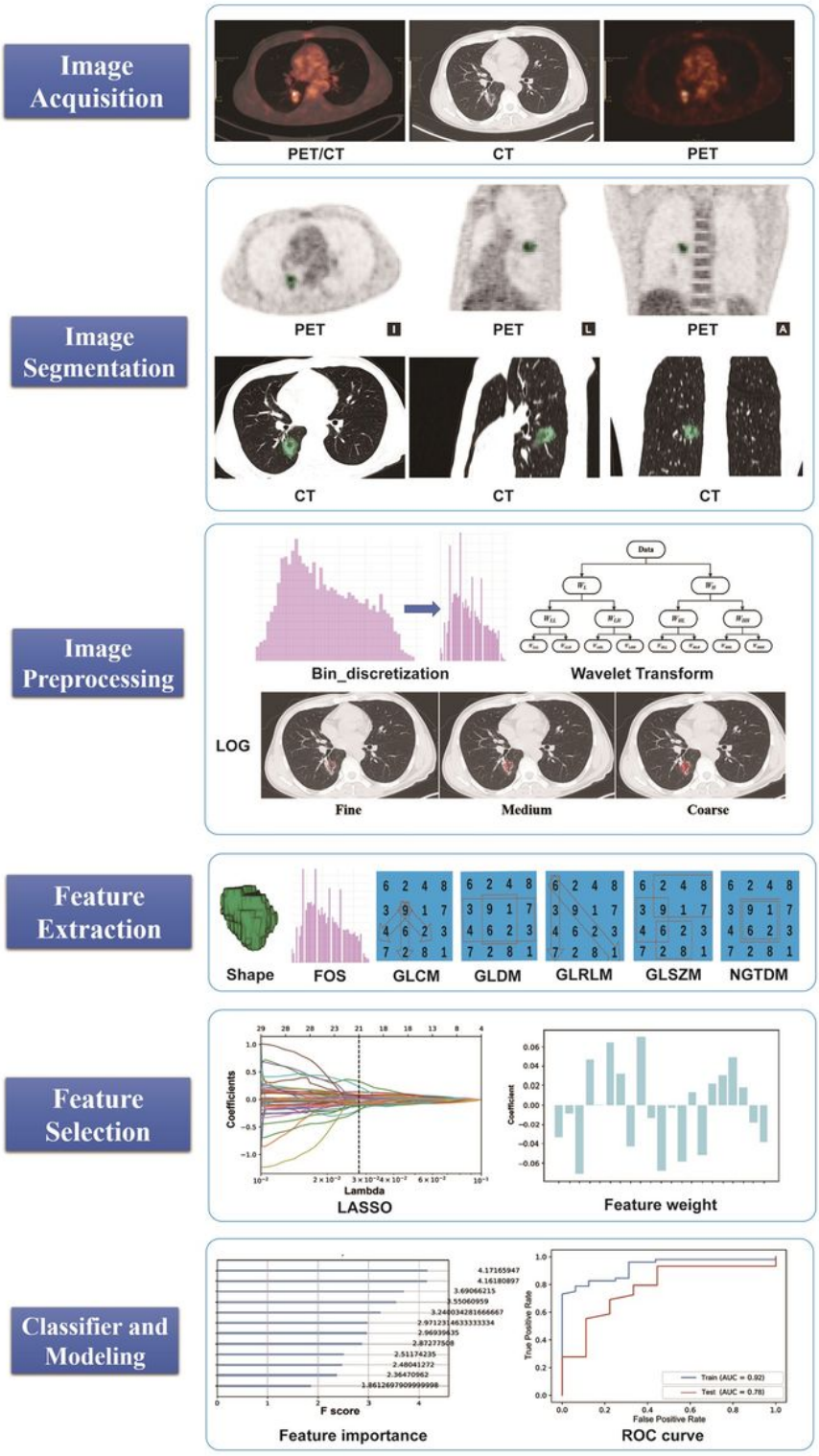

Figure 2

Flow chart of radiomics analysis

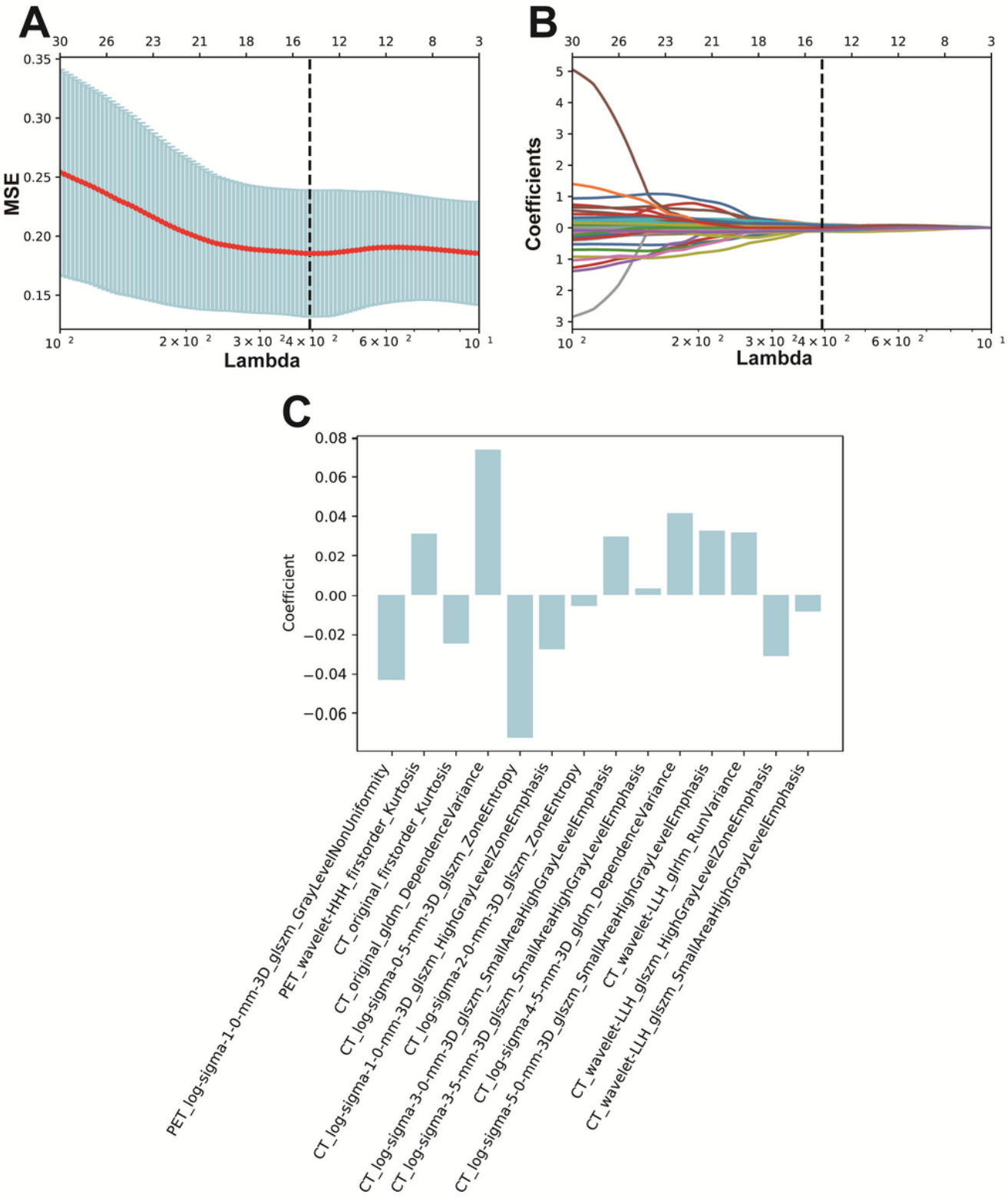

Figure 3

Extraction of the best subset of radiomic features using LASSO algorithm and 5-fold cross-validation. (A) Select the best feature based on the Mean Square Error (MSE) value. The black vertical line defines the best λ value, and the model provides the best fit of the data. λ=0.039. (B) LASSO coefficient distribution of the 55 radiomic features. The vertical line is the value selected by 5-fold cross-validation in A, where the best λ yields 14 nonzero coefficients of 21 selected features. (C) The weight map of 14 features

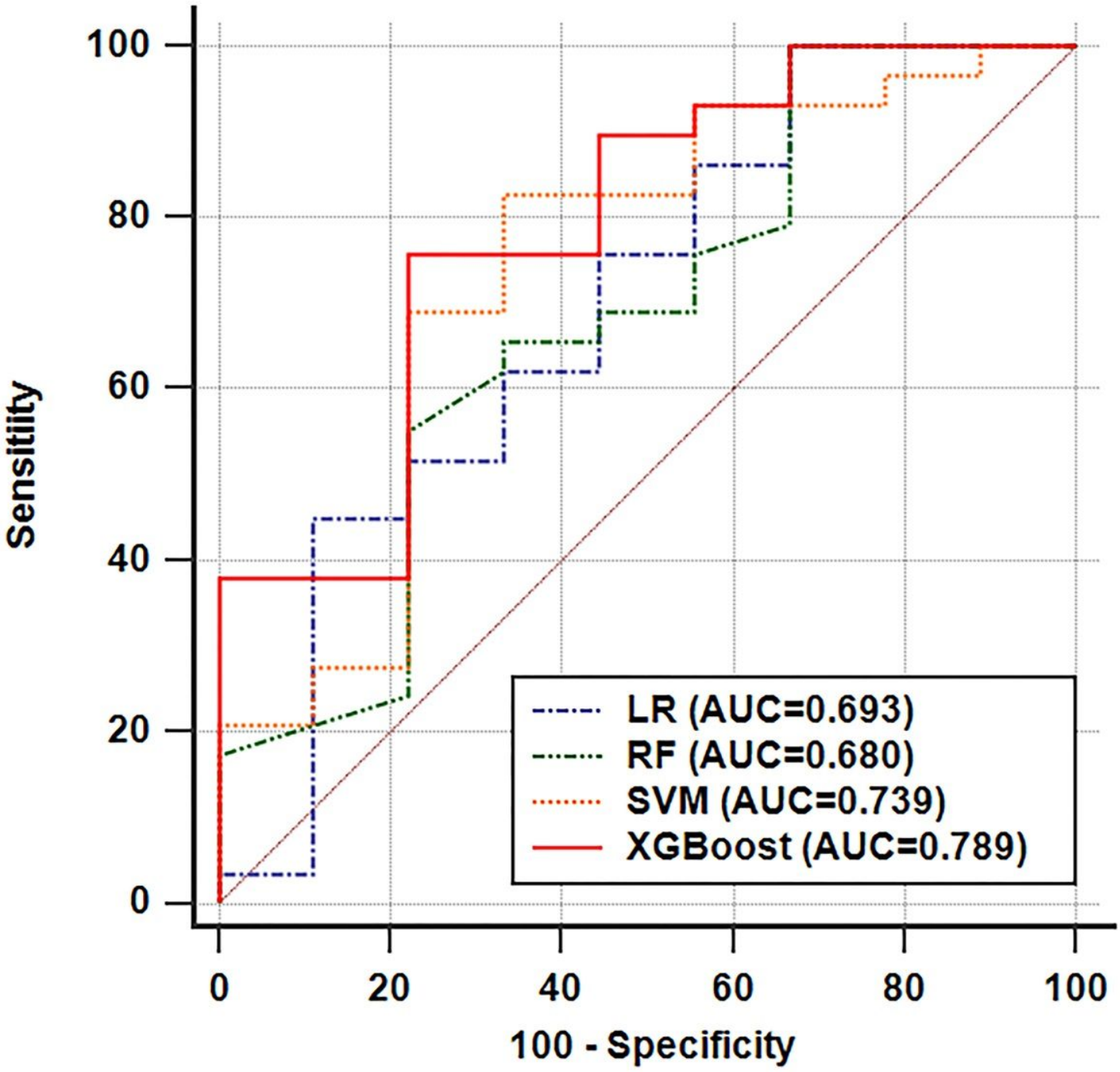

Figure 4

ROC curves of the four models on the testing set

Supplementary Files

This is a list of supplementary files associated with this preprint. Click to download.

- SupplementaryMaterial.doc